AGU PUBLICATIONS
JGR
Journal of Geophysical Research: Atmospheres

RESEARCH ARTICLE
10.1002/2017JD026501

Key Points:
- Monomethylamine, dimethylamine, and trimethylamines (MMA, DMA, and TMA) enhance H_2SO_4-driven particle formation but differ in their enhancing potentials
- Simulations indicate that clustering with H_2SO_4 is efficient for DMA and TMA and weaker and more sensitive to ambient conditions for MMA
- DMA and TMA can be approximated as a single surrogate species, but MMA cannot be assumed to behave similarly in terms of particle formation

Supporting Information:
- Supporting Information S1

Correspondence to:
T. Olenius,
tinja.olenius@alumni.helsinki.fi

Citation:
Olenius, T., R. Halonen, T. Kurtén, H. Henschel, O. Kupiainen-Määttä, I. K. Ortega, C. N. Jen, H. Vehkamäki, and I. Riipinen (2017), New particle formation from sulfuric acid and amines: Comparison of monomethylamine, dimethylamine, and trimethylamine, *J. Geophys. Res. Atmos.*, *122*, 7103–7118, doi:10.1002/2017JD026501.

Received 13 JAN 2017
Accepted 23 JUN 2017
Accepted article online 28 JUN 2017
Published online 12 JUL 2017

New particle formation from sulfuric acid and amines: Comparison of monomethylamine, dimethylamine, and trimethylamine

Tinja Olenius[1], Roope Halonen[2], Theo Kurtén[3], Henning Henschel[2,4], Oona Kupiainen-Määttä[2], Ismael K. Ortega[2,5], Coty N. Jen[6], Hanna Vehkamäki[2], and Ilona Riipinen[1]

[1]Department of Environmental Science and Analytical Chemistry (ACES) and Bolin Centre for Climate Research, Stockholm University, Stockholm, Sweden, [2]Department of Physics, University of Helsinki, Helsinki, Finland, [3]Department of Chemistry, University of Helsinki, Helsinki, Finland, [4]Now at Research Unit of Medical Imaging, Physics and Technology, University of Oulu, Oulu, Finland, [5]Now at ONERA-The French Aerospace Lab, Palaiseau, France, [6]Environmental Science, Policy, and Management, University of California, Berkeley, California, USA

Abstract Amines are bases that originate from both anthropogenic and natural sources, and they are recognized as candidates to participate in atmospheric aerosol particle formation together with sulfuric acid. Monomethylamine, dimethylamine, and trimethylamine (MMA, DMA, and TMA, respectively) have been shown to enhance sulfuric acid-driven particle formation more efficiently than ammonia, but both theory and laboratory experiments suggest that there are differences in their enhancing potentials. However, as quantitative concentrations and thermochemical properties of different amines remain relatively uncertain, and also for computational reasons, the compounds have been treated as a single surrogate amine species in large-scale modeling studies. In this work, the differences and similarities of MMA, DMA, and TMA are studied by simulations of molecular cluster formation from sulfuric acid, water, and each of the three amines. Quantum chemistry-based cluster evaporation rate constants are applied in a cluster population dynamics model to yield cluster concentrations and formation rates at boundary layer conditions. While there are differences, for instance, in the clustering mechanisms and cluster hygroscopicity for the three amines, DMA and TMA can be approximated as a lumped species. Formation of nanometer-sized particles and its dependence on ambient conditions is roughly similar for these two: both efficiently form clusters with sulfuric acid, and cluster formation is rather insensitive to changes in temperature and relative humidity. Particle formation from sulfuric acid and MMA is weaker and significantly more sensitive to ambient conditions. Therefore, merging MMA together with DMA and TMA introduces inaccuracies in sulfuric acid-amine particle formation schemes.

1. Introduction

Alkylamines, including monomethylamine (MMA), dimethylamine (DMA), and trimethylamine (TMA), are organic base compounds that are emitted to the atmosphere from various sources, such as animal husbandry, oceans, and biomass burning [*Ge et al*., 2011]. Although the concentrations of amines are significantly lower than ammonia, they are still among the most abundant atmospheric bases [*Ge et al*., 2011]. Due to their higher basicity, amines are likely to bind to sulfuric acid molecules more efficiently than ammonia [*Qiu and Zhang*, 2013] and have recently been shown by various studies to influence new particle formation (NPF) processes involving sulfuric acid. Despite their potential importance for atmospheric aerosol formation, quantitative estimates on the emissions, concentrations, and thermochemical properties of atmospheric amines are still relatively uncertain. As a result, recent large-scale modeling studies have treated amines through the introduction of a single surrogate amine species, whose total emissions combine together MMA, DMA, and TMA but which resembles DMA or TMA in its various properties [see, e.g., *Bergman et al*., 2015]. In conditions where atmospheric concentrations of amines are elevated due to, e.g., application of carbon sequestration techniques involving amines [*Belman et al*., 2009], it is important to evaluate the validity of the surrogate approach.

A number of theoretical studies have focused on examining the stabilities of small molecular clusters of sulfuric acid and amines by calculations of the thermodynamic properties of the clusters with quantum chemical methods. *Kurtén et al*. [2008] first concluded that different amine species generally stabilize

sulfuric acid clusters considerably more efficiently than ammonia. Similar results on the stabilities of acid-ammonia and acid-dimethylamine clusters of a few molecules have been obtained since by, for instance, *Loukonen et al*. [2010], *Nadykto et al*. [2011], *Ortega et al*. [2012], and *DePalma et al*. [2014]. While the quantitative results of quantum chemical calculations performed at different levels of theory may somewhat vary (see, e.g., *Leverentz et al*. [2013] and *Kupiainen-Määttä et al*. [2013] for method comparisons), the qualitative results point to atmospheric amines being likely to form stable clusters with sulfuric acid.

Several laboratory studies conducted using particle counters have recently addressed particle formation in the presence of amines. *Erupe et al*. [2011] and *Yu et al*. [2012] observed elevated ~2 nm particle concentrations upon the addition of trimethylamine or dimethylamine to sulfuric acid and water vapors in a flow tube setup. *Almeida et al*. [2013] deduced particle formation rates from particle concentration measurements in a chamber experiment and showed that dimethylamine can increase the formation rate by more than 3 orders of magnitude compared to ammonia. *Glasoe et al*. [2015] studied particle formation in a flow tube using sulfuric acid, water, and different bases including ammonia and amines. The measured particle concentrations indicated that the relative efficiency of the bases to form particles with sulfuric acid increases from ammonia as the weakest, to monomethylamine as the next, and finally to dimethylamine and trimethylamine as the strongest stabilizers.

Comparing particle counter measurements to predictions of cluster stabilities is, however, not straightforward: counters mainly detect clusters larger than what can be studied with quantum chemistry and do not provide direct information on the cluster composition. Instead, high-resolution mass spectrometers can be used to determine the elemental composition of electrically charged clusters down to single molecules, and the same methods can be used for electrically neutral clusters by combining a chemical ionization unit with a mass spectrometer [see, e.g., *Zhao et al*., 2011; *Kürten et al*., 2014]. *Kürten et al*. [2014] were able to detect a spectrum of electrically neutral molecular clusters containing up to 14 acid and 16 dimethylamine molecules in a chamber experiment involving sulfuric acid, dimethylamine, and water. *Jen et al*. [2014] performed flow tube measurements on sulfuric acid-base-water systems, where the base was either ammonia or monomethylamine, dimethylamine, or trimethylamine. They measured the concentration of neutral clusters containing two sulfuric acid molecules stabilized by base molecules at different acid and base vapor concentrations at fixed temperature and relative humidity and reported the same relative stabilization efficiencies for the bases as *Glasoe et al*. [2015]. The mass spectrometer technique can, however, affect the composition of especially the smallest clusters, which may lose one or more molecules while being charged or via possible fragmentation processes inside the instrument [*Zhao et al*., 2011; *Kürten et al*., 2014; *Ortega et al*., 2014]. Specifically, sulfuric acid dimers are likely to lose all base and water molecules upon chemical ionization using nitrate [*Jen et al*., 2014].

Finally, a direct comparison between theory and observations is not possible solely via predictions on cluster stabilities: quantum chemical approaches probe the properties of individual clusters, while NPF experiments principally address cluster concentrations that result from the combination of all dynamic processes involving the clusters and vapor molecules. Connecting the predictions with measurable quantities thus requires modeling a population of clusters considering collisions, evaporations, vapor sources, attachment of clusters to surfaces, and possibly other processes depending on the situation. Quantum chemical results can be used in cluster population modeling for obtaining cluster evaporation rate constants, which can be calculated from the formation free energies and collision rate constants. Cluster populations have been modeled in such a manner for sulfuric acid, ammonia, and/or dimethylamine by, e.g., *Kupiainen et al*. [2012], *Olenius et al*. [2013], and *Almeida et al*. [2013], showing that dimethylamine forms clusters with acid more efficiently than ammonia and leads to higher particle formation rates.

To summarize, dimethylamine has hitherto been the most studied atmospheric amine. While other similar amine species have been assumed to have comparable average properties with respect to clustering [e.g., *Loukonen et al*., 2010; *Bergman et al*., 2015], both experimental [*Jen et al*., 2014; *Glasoe et al*., 2015] and theoretical [*Kurtén et al*., 2008; *Paasonen et al*., 2012] studies suggest that there may be differences between the stabilization potentials of different alkylamines at least for the smallest clusters. Systematic comparisons of different amine species are scarce, but they are needed to assess how to treat this complex array of species in atmospheric models. In this work, the capabilities of monomethylamine, dimethylamine, and trimethylamine to bind to small electrically neutral sulfuric acid clusters are examined using consistent

computational methods. Previously published quantum chemical data sets of sulfuric acid-amine-water clusters are complemented with additional clusters and hydrates for monomethylamine and trimethylamine, and the quantum chemistry-based cluster evaporation rate constants are implemented in a parameter-free dynamic cluster population model to study the cluster distributions and growth kinetics at different ambient conditions. First, we consider a situation corresponding to the experiment by *Jen et al*. [2014]. We demonstrate a good agreement between the modeled and observed cluster concentrations and proceed by simulating the cluster populations in a set of conditions relevant to the atmosphere, where the sulfuric acid concentration is generally lower than in the flow tube experiment, and the temperature and relative humidity cover a range of typical values. We present results on sulfuric acid-amine clustering in the form of observable quantities and discuss the similarities and differences of the three alkylamines. We aim to address the following question: Can these species be approximated as a single surrogate amine, and if not, what kind of effects can the surrogate assumption have?

2. Methods

We study three sets of sulfuric acid-amine molecular clusters, where the amine is monomethylamine, dimethylamine, or trimethylamine, henceforth abbreviated as MMA, DMA, and TMA, respectively. Simulations of acid-ammonia clusters are also shown for comparison. The simulation systems cover cluster sizes containing up to *n* H_2SO_4 and *n* base molecules hydrated by 0–5 water molecules, where *n* is 5 for NH_3, 3 for MMA, 4 for DMA, and 2 for TMA. The system sizes are slightly different for the different base species, as more weakly bound systems require including larger clusters in the simulation, and due to computational reasons, water molecules are not included in some of the largest clusters. All studied clusters are listed in Table S1 in the supporting information. The electronic energies and thermochemical parameters of the clusters were first computed with quantum chemical methods. The data were then implemented in a dynamic cluster distribution model as cluster evaporation rate constants calculated from the Gibbs free energies of formation.

2.1. Quantum Chemical Calculations

Thermochemical data for H_2SO_4-amine clusters were computed with a quantum chemical multistep method described by *Ortega et al*. [2012]. The method uses the B3LYP functional with a CBSB7 basis set for geometry optimizations and vibrational frequency calculations (performed with Gaussian09) [*Frisch et al*., 2009] and the RICC2 method with an aug-cc-pV(T+d)Z basis set for single point energies (calculated with Turbomole) [*Ahlrichs et al*., 1989]. Data for NH_3 and DMA, as well as few MMA and TMA clusters, have been published previously in our other works [*Olenius et al*., 2013, 2014; *Henschel et al*., 2014, 2016], and in this work the data sets were completed for MMA and TMA.

As there can be significant differences in the quantitative energy values calculated at different quantum chemical levels of theory, the electronic energies of the smallest clusters consisting of one H_2SO_4 and one base molecule were computed also at the RHF, MP2-F12, CCSD-F12a, and CCSD(T)-F12a levels (with Molpro 2012.1) [*Werner et al*., 2012] using either the VDZ-F12 or VTZ-F12 basis set in order to assess uncertainties related to the initial clustering. Moreover, we performed clustering simulations also using thermochemical data published by *Nadykto et al*. [2014], where all quantities have been computed using the PW91PW91 functional with the 6-311++G(3df) basis set.

2.2. Cluster Population Modeling

We used the Atmospheric Cluster Dynamics Code to simulate the kinetics of molecular clusters populations. The code generates and solves the cluster birth-death equations, that is, the time derivatives of the cluster concentrations to obtain the time development of the concentrations of all clusters included in the simulation [see, e.g., *Olenius et al*., 2013; *Henschel et al*., 2016]. The time derivatives include all possible collision and evaporation processes between the simulated clusters and molecules, as well as possible external source and sink terms. The collision rate constants were calculated from the kinetic gas theory assuming spherical clusters with the radii calculated from the molecular masses (18.02, 98.08, 17.04, 31.06, 45.08, and 59.11 g mol^{-1} for H_2O, H_2SO_4, NH_3, MMA, DMA, and TMA, respectively) and liquid densities (997, 1830, 696, 656, 680, and 627 kg m^{-3} for H_2O, H_2SO_4, NH_3, MMA, DMA, and TMA, respectively, mostly determined at 20–25°C [see *Haynes*, 2014]) of the pure compounds assuming ideal mixing. The evaporation rate

constants were calculated from the Gibbs free energies of formation of the clusters according to the concept of detailed balance [see, e.g., *Ortega et al*., 2012]. Explicit numerical treatment of coupled kinetic processes with extremely large differences in the rate constants is often in practice impossible. For the molecular systems of this work, such differences originate from the collision and evaporation rate constants of water, which are approximately 10 orders of magnitude higher than those of the other compounds. Therefore, sulfuric acid and base molecules and acid-base clusters were considered explicitly in the simulations, and water was treated implicitly by assuming equilibrium hydrate distributions for all the molecules and clusters. This means that instead of, for instance, assuming some average water content for the clusters, each hydrate containing a different number of water molecules is considered, but the water equilibration is assumed to occur instantaneously for each time step [see *Henschel et al*., 2016]. When a collision resulted in a cluster outside of the simulated size range, the cluster was let to grow out of the system if its composition could be considered relatively stable (see supplementary information); otherwise, the cluster was brought back to the simulation system by monomer evaporations. The cluster growth pathways were tracked as described by *Olenius et al*. [2013].

The flux of clusters growing successfully out of the $n \times n$ simulation system, where n is the maximum number of H_2SO_4 and base molecules in the studied clusters (see Table S1), was recorded as the formation rate J. The particle size corresponding to the formation rate is slightly different for the different base systems: the approximate mass diameter of the outgrowing clusters is ~1.1 nm for NH_3 (corresponding to a molecular content of at least six H_2SO_4, five NH_3, and any number of H_2O molecules; see section 1 in the supporting information and Figure 3), 1.0 nm for MMA ($\geq$4 H_2SO_4 and $\geq$3 MMA molecules), 1.2 nm for DMA ($\geq$5 H_2SO_4 and $\geq$4 DMA molecules or $\geq$4 H_2SO_4 and $\geq$5 DMA molecules), and 1.4 nm for TMA ($\geq$3 H_2SO_4 and $\geq$2 TMA molecules). As the formation rate cannot be directly measured, we also present the total concentration $\sum[(H_2SO_4)_2]$ of clusters consisting of two H_2SO_4 molecules and any number of base and water molecules as a representative measurable quantity characterizing the stabilization potential of the different bases. The dimer concentration $\sum[(H_2SO_4)_2]$ has recently been measured in different types of laboratory [*Almeida et al*., 2013; *Jen et al*., 2014] and field [*Kürten et al*., 2016] experiments.

The cluster populations were modeled in two different situations: a time-dependent situation corresponding to a laminar flow tube and a time-independent steady state in conditions relevant to the atmospheric boundary layer.

2.2.1. Laminar Flow Tube Simulations

The simulation setup mimicking the conditions of a laminar flow tube is similar to that described by *Olenius et al*. [2014]. In this work, the vapor concentrations and diffusion loss constants were set to correspond to the experimental conditions of *Jen et al*. [2014]. Their measurements were conducted using a flow tube with an inner radius of 2.5 cm at a total pressure of 0.97 atm. The temperature was maintained at 295–305 K and the relative humidity at 30%. Base vapor was injected to the sulfuric acid-containing flow of humidified nitrogen gas along the centerline of the tube, after which dilution mixing decreased the centerline base concentration. The concentrations of clusters containing one and two sulfuric acid molecules with any number of base and water molecules were then measured with a chemical ionization mass spectrometer at the end of the tube. The measured sulfuric acid concentration ranged from approximately 10^7 to 10^9 cm^{-3}, and the base concentration varied between a few and ~200–300 parts per trillion (ppt) (~10^7–10^8 cm^{-3} … $5 \cdot 10^9$–$7 \cdot 10^9$ cm^{-3}) for amines and between 100 and 6000 ppt ($2 \cdot 10^9$ … 10^{11} cm^{-3}) for ammonia.

In the simulations, sulfuric acid and base vapors were set to have initial concentrations corresponding to the base injection point in the flow tube, after which the vapor and cluster concentrations were allowed to evolve as the air parcel travels through the tube. The simulation does not resolve the 2-D or 3-D flow, but corresponds to the central streamline, around which radial concentration gradients are assumed to be small. Due to the short equilibrium time scales of water, losses of water vapor were neglected and the relative humidity was assumed to have a fixed value throughout the simulation. The time development of the cluster distribution along the central streamline was simulated at 298.15 K for the residence time of 3 s reported for the flow tube.All clusters and molecules apart from water were assumed to be lost on the walls of the flow tube at a diffusion-limited loss frequency $k_{\mathrm{wall},i}$ (s^{-1}) calculated as [see, e.g., *Olenius et al*., 2014]

$$k_{\mathrm{wall},i} = \frac{3.65 D_{i,\mathrm{N_2}}}{r^2}, \tag{1}$$

where D_{i,N_2} ($m^2\ s^{-1}$) is the diffusion coefficient of species i in nitrogen gas, r (m) is the inner radius of the flow tube (here 2.5 cm), and subscript i refers to a specific cluster or molecule. The diffusion coefficients were calculated from the kinetic gas theory as

$$D_{i,N_2} = \frac{3}{8}\frac{(k_B T)^{3/2}}{P_{tot}(r_i + r_{N_2})^2}\left[\frac{1}{2\pi}\left(\frac{1}{m_i}+\frac{1}{m_{N_2}}\right)\right]^{1/2}, \quad (2)$$

where k_B is the Boltzmann constant, T is the temperature, P_{tot} is the total pressure in the flow tube (here 0.97 atm), and r_i and m_i are the radius and mass of cluster or molecule i and r_{N_2} and m_{N_2} those of the nitrogen molecule. The radii of the studied clusters and molecules were calculated from the masses and bulk densities of the compounds, and the radius of the nitrogen molecule r_{N_2} was assumed to depend on the viscosity η_{N_2} of pure nitrogen gas as

$$r_{N_2} = \frac{1}{2}\left(\frac{5}{16\eta_{N_2}}\right)^{1/2}\left(\frac{m_{N_2}k_B T}{\pi}\right)^{1/4}. \quad (3)$$

The temperature-depend viscosity was calculated according to the Sutherland formula based on a reference value of $\eta_{N_2,0}$ = 17.8771 Pa s at T_0 = 300 K [*Lemmon and Jacobsen*, 2004] as

$$\eta_{N_2} = \eta_{N_2,0}\left(\frac{T_0 + C}{T + C}\right)\left(\frac{T}{T_0}\right)^{3/2}, \quad (4)$$

where the constant C for nitrogen is 111 K [*Crane*, 1982].

In the setup of *Jen et al*. [2014], the base vapor is injected separately to the flow and is therefore expected to have higher losses from the central streamline due to radial dilution. *Jen et al*. [2014] estimated the centerline base concentration at the injection point to be approximately 10 times higher than at the detection point. We thus tested different initial base concentrations and a higher loss frequency from the centerline for the base molecules than for the other species (see supporting information).

2.2.2. Steady State Simulations Corresponding to the Atmosphere

The second simulation setup considers a time-independent steady state situation at different vapor concentrations, relative humidities, and temperatures representative of conditions in the lower atmosphere. Evaporation rate constants of individual clusters depend on temperature and hydration, which motivates studies on the cluster populations at different temperatures and relative humidities. Furthermore, the role of evaporation becomes more significant as the absolute vapor concentrations decrease, and the sulfuric acid concentration relevant to atmospheric NPF events is often down to an order of magnitude lower than the lowest concentrations of the flow tube experiment by *Jen et al*. [2014]. The exact concentrations of atmospheric amines are not well known, but depending on the location, they may also have values lower than those included in the experimental range [*Ge et al*., 2011]. The relative contributions of collisions and evaporations also vary as the cluster population evolves in time. Typical time scales of variations in the ambient conditions in the atmosphere are of the order of minutes to hours, which is considerably longer than the flow tube residence time. While the temporal variability may be prominent also in the atmosphere, the time to reach the steady state at a constant vapor production rate is relatively short for the smallest cluster sizes, often of the order of ~30 min. Thus, the steady state was chosen as a simplified representative situation to examine the effects of different atmospheric conditions. The sulfuric acid concentration (referring to the measurable concentration, i.e., the sum of all clusters containing one acid molecule and any number of base and water molecules) was set to 10^6–10^8 cm^{-3}, and the amine or ammonia concentration to 0.1–100 ppt (~$3 \cdot 10^6$–$3 \cdot 10^9$ cm^{-3}), depending on the base. The temperature was varied between 260 and 300 K and the relative humidity between 0 and 100%.An external sink corresponding to scavenging by a preexisting population of larger particles was used for all clusters and molecules. As proposed by *Lehtinen et al*. [2007], the coagulational loss frequency $k_{coag,i}$ (s^{-1}) was approximated to depend on the cluster radius r_i according to the power law

$$k_{coag,i} = k_{coag,ref}\left(\frac{r_i}{r_{ref}}\right)^m, \quad (5)$$

where $k_{coag,ref}$ is the loss rate constant of a reference size r_{ref} and m is a constant. The sulfuric acid molecule was used as the reference size, and its loss frequency was set to 10^{-3} s^{-1} based on observations in boreal

Table 1. Electronic Energies (ΔE_{elec}), Enthalpies ($\Delta H_{298.15\ K}$), Gibbs Free Energies ($\Delta G_{298.15\ K}$), and Entropies ($\Delta S_{298.15\ K}$) of Formation From Monomers Computed at the RICC2/aug-cc-pV(T+d)Z//B3LYP/CBSB7 Level of Theory for H_2SO_4-MMA and H_2SO_4-TMA Clusters and Their Hydrates[a]

Cluster	ΔE_{elec} (kcal mol^{-1})	$\Delta H_{298.15\ K}$ (kcal mol^{-1})	$\Delta G_{298.15\ K}$ (kcal mol^{-1})	$\Delta S_{298.15\ K}$ (cal K^{-1} mol^{-1})
		H_2SO_4-MMA Clusters		
CH_3NH_2•H_2O	−7.34	−5.40	2.55	−26.66
CH_3NH_2•$(H_2O)_2$	−17.03	−13.15	4.19	−58.15
H_2SO_4•CH_3NH_2	−22.83	−20.82	−11.46	−31.36
H_2SO_4•CH_3NH_2•H_2O	−38.41	−34.10	−13.74	−68.29
H_2SO_4•CH_3NH_2•$(H_2O)_2$	−53.04	−46.85	−18.13	−96.32
H_2SO_4•CH_3NH_2•$(H_2O)_3$[b]	−65.17	−57.07	−20.07	−124.09
$(H_2SO_4)_2$•CH_3NH_2	−56.47	−52.54	−30.39	−74.31
$(H_2SO_4)_2$•CH_3NH_2•H_2O	−69.55	−63.65	−32.44	−104.69
$(H_2SO_4)_2$•CH_3NH_2•$(H_2O)_2$	−81.67	−74.12	−33.75	−135.41
$(H_2SO_4)_2$•CH_3NH_2•$(H_2O)_3$	−97.54	−88.38	−36.06	−175.48
$(H_2SO_4)_3$•CH_3NH_2	−81.57	−76.22	−42.43	−113.32
H_2SO_4•$(CH_3NH_2)_2$	−38.17	−35.23	−16.36	−63.31
H_2SO_4•$(CH_3NH_2)_2$•H_2O	−53.98	−48.48	−19.13	−98.45
H_2SO_4•$(CH_3NH_2)_2$•$(H_2O)_2$	−68.92	−61.27	−22.29	−130.74
$(H_2SO_4)_2$•$(CH_3NH_2)_2$	−83.11	−76.23	−44.23	−107.34
$(H_2SO_4)_2$•$(CH_3NH_2)_2$•H_2O	−100.09	−91.04	−48.36	−143.18
$(H_2SO_4)_2$•$(CH_3NH_2)_2$•$(H_2O)_2$	−115.45	−104.42	−51.24	−178.36
$(H_2SO_4)_2$•$(CH_3NH_2)_2$•$(H_2O)_3$	−128.24	−115.23	−51.86	−212.55
$(H_2SO_4)_2$•$(CH_3NH_2)_2$•$(H_2O)_4$	−140.01	−125.17	−53.13	−241.64
$(H_2SO_4)_3$•$(CH_3NH_2)_2$	−114.79	−106.30	−61.77	−149.36
H_2SO_4•$(CH_3NH_2)_3$	−55.63	−50.13	−18.89	−104.75
$(H_2SO_4)_2$•$(CH_3NH_2)_3$	−99.92	−91.39	−48.45	−144.03
$(H_2SO_4)_3$•$(CH_3NH_2)_3$	−148.31	−136.78	−80.35	−189.26
		H_2SO_4-TMA Clusters		
$(CH_3)_3N$•H_2O	−8.19	−6.27	1.81	−27.11
H_2SO_4•$(CH_3)_3N$	−28.49	−26.04	−15.74	−34.54
H_2SO_4•$(CH_3)_3N$•H_2O[b]	−40.52	−36.10	−16.58	−65.45
H_2SO_4•$(CH_3)_3N$•$(H_2O)_2$[b]	−53.28	−46.80	−16.84	−100.51
H_2SO_4•$(CH_3)_3N$•$(H_2O)_3$	−67.24	−58.51	−17.49	−137.58
$(H_2SO_4)_2$•$(CH_3)_3N$	−57.86	−53.24	−31.27	−73.70
$(H_2SO_4)_2$•$(CH_3)_3N$•H_2O	−70.50	−64.50	−32.98	−105.71
$(H_2SO_4)_2$•$(CH_3)_3N$•$(H_2O)_2$	−86.35	−78.44	−34.88	−146.09
$(H_2SO_4)_2$•$(CH_3)_3N$•$(H_2O)_3$	−98.01	−88.15	−34.79	−178.98
H_2SO_4•$((CH_3)_3N)_2$	−45.79	−42.23	−20.87	−71.66
H_2SO_4•$((CH_3)_3N)_2$•H_2O	−58.86	−52.46	−21.82	−102.79
H_2SO_4•$((CH_3)_3N)_2$•$(H_2O)_2$	−70.21	−61.79	−22.07	−133.21
$(H_2SO_4)_2$•$((CH_3)_3N)_2$	−92.65	−84.48	−49.17	−118.41
$(H_2SO_4)_2$•$((CH_3)_3N)_2$•H_2O	−96.71	−87.30	−43.61	−146.53
$(H_2SO_4)_2$•$((CH_3)_3N)_2$•$(H_2O)_2$	−110.36	−98.98	−46.98	−174.41
$(H_2SO_4)_2$•$((CH_3)_3N)_2$•$(H_2O)_3$	−121.71	−107.72	−44.20	−213.05

[a]Data for H_2SO_4–DMA and H_2SO_4–NH_3 clusters can be found in the works of *Olenius et al.* [2013] and *Henschel et al.* [2014, 2016]. All values are at 298.15 K and 1 atm reference pressure.
[b]Values published in our previous work [*Olenius et al.*, 2014] replaced after finding a more stable structure.

environments [*Dal Maso et al.*, 2008]. *m* was assumed to be −1.7, as determined for a similar environment by *Lehtinen et al.* [2007].

3. Results and Discussion

Cluster formation energies of H_2SO_4-MMA-H_2O and H_2SO_4-TMA-H_2O clusters obtained at the RICC2/aug-cc-pV(T+d)Z//B3LYP/CBSB7 level of theory are presented in Table 1; data for H_2SO_4-NH_3-H_2O and H_2SO_4–DMA–H_2O clusters are given in the works by *Henschel et al.* [2014, 2016]. The energies of the first hydrates of the H_2SO_4•MMA cluster found here are similar to those reported by *Bustos et al.* [2014], *Lv et al.* [2015], and *Nadykto et al.* [2011], except for that our calculations suggest the first hydration step to be less exergonic

Table 2. Binding Energies (Electronic Energies of Formation, Not Including Zero-Point Vibrational Contributions, in kcal/mol) of H_2SO_4•Base Clusters at Various Levels of Theory and Using Either the VDZ-F12 ("VDZ") or VTZ-F12 ("VTZ") Basis Sets

		Method				
Cluster	Basis Set	RHF	MP2-F12[a]	CCSD-F12a	CCSD(T)-F12a	RICC2/aug-cc-pV(T+d)Z
H_2SO_4•NH_3	VDZ	−11.40	−16.91	−15.47	−16.27	−17.39
	VTZ	−11.13	−16.87	−15.42	−16.33	
H_2SO_4• CH_3NH_2	VDZ	−12.58	−21.76	−19.01	−20.30	−22.83
	VTZ	−12.56	−21.82	−19.09	−20.59	
H_2SO_4•$(CH_3)_2NH$	VDZ	−16.63	−25.67	−22.99	−24.34	−27.22
	VTZ	−16.37	−25.68	−23.03	−24.56	
H_2SO_4•$(CH_3)_3N$	VDZ	−17.26	−26.48	−23.78	−25.18	−28.49
	VTZ	−16.56	−26.46	−23.78	–	

[a]DF-MP2-F12 using the 3C(FIX) ansatz.

than reported in these previous articles. For the hydration of the $(H_2SO_4)_2$•MMA and the H_2SO_4•TMA cluster our calculations yield somewhat more negative free energies as compared to *Lv et al*. [2015] and *Nadykto et al*. [2011], respectively.

In general, the free energies of hydration of the MMA-containing clusters are very similar to those previously reported for ammonia-containing clusters [*Henschel et al*., 2014]. The H_2SO_4•MMA is somewhat more and the $(H_2SO_4)_2$•MMA slightly less hydrophilic compared to the corresponding ammonia-containing cluster: for instance, at 278 K and RH $>$ 20%, the average number of water molecules is ~2–2.5 for H_2SO_4•MMA and ~1.5–2 for H_2SO_4•NH_3 (Figure S3 in the supporting information). For the $(H_2SO_4)_2$•base cluster, the average water content increases steadily to ~1 for MMA and to ~2 for NH_3 as RH increases from 0 to 100%. The free energies of hydration of the TMA-containing clusters follow a pattern very similar to that of the previously described DMA-containing clusters [*Henschel et al*., 2014]. Hydration of TMA-containing clusters is in most cases even less favorable than for the corresponding DMA clusters (and in most cases by more than 1.5 kcal/mol). Only the second hydration step of both the $(H_2SO_4)_2$•TMA and the $(H_2SO_4)_2$•TMA_2 cluster is by 1.5 kcal/mol more favorable than the corresponding hydration step in the sulfuric acid-DMA system. At 278 K and RH = 0–100%, the average water contents of H_2SO_4•TMA and H_2SO_4•DMA increase to ~0.1 and ~1.5, respectively, and those of $(H_2SO_4)_2$•TMA and $(H_2SO_4)_2$•DMA to ~1 (Figure S3). The $(H_2SO_4)_2$•$(DMA/TMA)_2$ clusters remain in practice unhydrated.

Table 2 shows the electronic energies computed for the unhydrated H_2SO_4•base complexes using a variety of wave function-based methods and either the VDZ-F12 or VTZ-F12 basis sets, with the RICC2/aug-cc-pV(T+d)Z values also given for reference. (For the H_2SO_4•TMA cluster, the CCSD(T)-F12/VTZ-F12 calculation was unfortunately computationally too demanding.) Note that all binding energies have been evaluated using the same (B3LYP/CBSB7) geometries. Several patterns can be discerned from Table 2. First, quantitatively accurate binding energies clearly require high-level treatment of electron correlation. For most cluster and basis set combinations, the differences between the most accurate CCSD(T)-F12a values on one hand, and the less accurate CCSD-F12a or MP2-F12 values on the other hand, are on the order of 1 kcal/mol (with a maximum difference of 1.5 kcal/mol). CCSD consistently underestimates the binding energy (i.e., inclusion of the perturbative triples contribution strengthens the binding), while MP2-F12 consistently overestimates it. RICC2/aug-cc-pV(T+d)Z behaves similarly to MP2-F12, but the degree of overbinding compared to the best available CCSD(T) results is stronger, about 1 kcal/mol for the H_2SO_4•NH_3 complex and 2–3 kcal/mol for the amines.

Second, the difference between results obtained with the two different basis sets (VDZ-F12 and VTZ-F12) is fairly small for all three explicitly correlated methods. Most importantly, the difference between the CCSD(T)-F12a/VDZ-F12 and CCSD(T)-F12a/VTZ-F12 binding energies is less than 0.3 kcal/mol for the three clusters for which the latter value could be computed. This indicates (as expected from previous studies on other hydrogen-bonded clusters [see, e.g., *Lane and Kjaergaard*, 2009]) that the CCSD(T)-F12a/VTZ-F12 binding energies are close to the CCSD(T) basis set limit—which in turn should be accurate to within ~1 kcal/mol or better for these electronically well-behaved closed-shell systems [*Karton*, 2016]. The effect of the density functional and basis set used for the geometry optimization on the coupled-cluster binding energies is likely to be quite small [*Myllys et al*., 2016]. However, the accuracy of the free energies may be lower than that

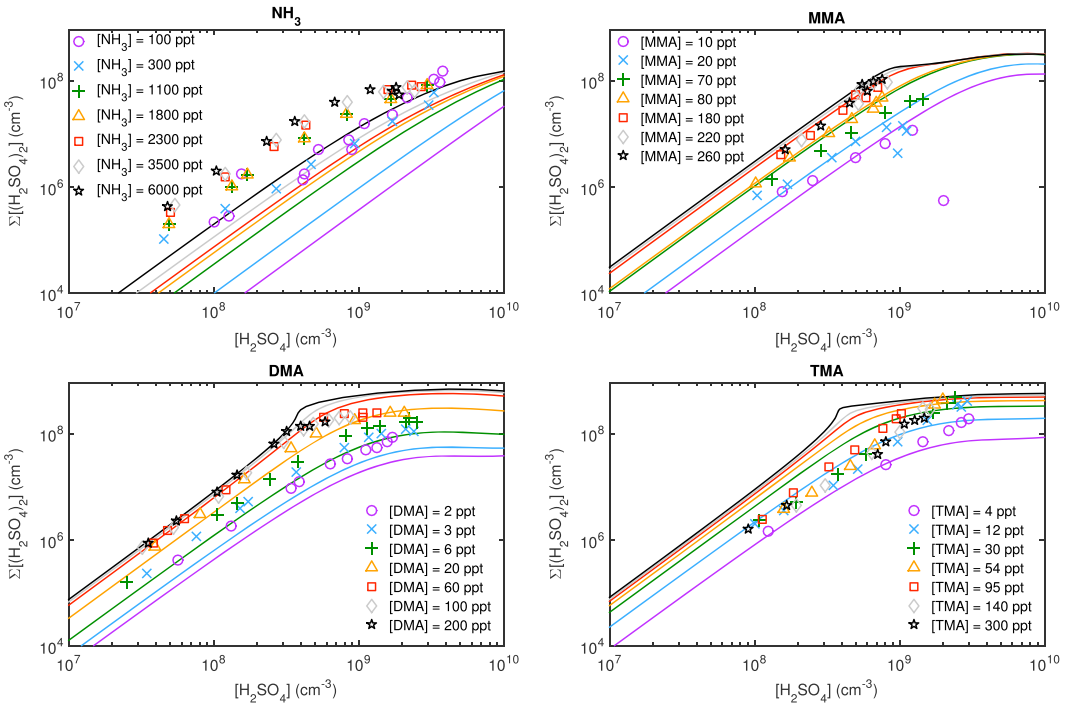

Figure 1. Simulated dimer concentration as a function of monomer concentration in a flow tube after a residence time of 3 s at RH = 30% (solid lines), obtained using the reported base concentration given in the legend. The symbols represent the experimental values reported by *Jen et al*. [2014]. Monomer and dimer concentrations are defined as the total concentrations of clusters containing one and two H_2SO_4 molecules, respectively, and any number of base and water ligands.

indicated by the CCSD(T) electronic energy calculations due to errors in the thermal contributions computed using the rigid rotor and harmonic oscillator approximations, especially for the entropy contributions.

Third, the relative stability of the four different clusters is well predicted already by quite modest (e.g., MP2-F12/VDZ-F12) levels of theory. All method/basis set combinations, including RICC2/aug-cc-pV(T+d)Z, predict the correct order of the H_2SO_4•base cluster stabilities. Quantitatively, the difference between the ammonia-containing and the amine-containing clusters is overestimated by MP2-F12 and RICC2 and underestimated by CCSD.

A comparison of RICC2 and CCSD(T) results thus indicate that as suggested previously [e.g., *Leverentz et al*., 2013], the former method predicts somewhat too strong binding for sulfuric acid-amine clusters and also somewhat exaggerates the differences between different bases (e.g., amines versus NH_3 or DMA/TMA versus MMA). Thus, the results presented here for sulfuric acid-base particle formation should be considered likely upper limits both with respect to the formation rates for any particular base and with respect to the quantitative differences predicted between different bases. However, the qualitative differences between different bases are likely correctly predicted, as demonstrated by Table 2.

3.1. Comparison to Experimental Flow Tube Data

Figure 1 presents the comparison of the simulated H_2SO_4 dimer concentrations, i.e., the sums of concentrations of all clusters consisting of two H_2SO_4 molecules and any numbers of water and one of the four bases, to the flow tube measurements by *Jen et al*. [2014]. Figure 1 shows simulations performed with initial base concentrations corresponding to the reported observed concentrations, and results for higher initial base concentrations and approximative additional dilution losses for the base vapor are given in Figure S15. The overall agreement is good: the trends and relative concentrations are mostly reproduced by the simulations. The effect of the base vapor concentration is generally somewhat larger for the model data than for the experiments, and for the H_2SO_4-NH_3 system, the absolute dimer concentrations are underestimated for all [NH_3]. The MMA case shows the best agreement between the simulation and measurement in the absolute values: the dependence of the dimer concentration on both sulfuric acid and MMA concentrations is well

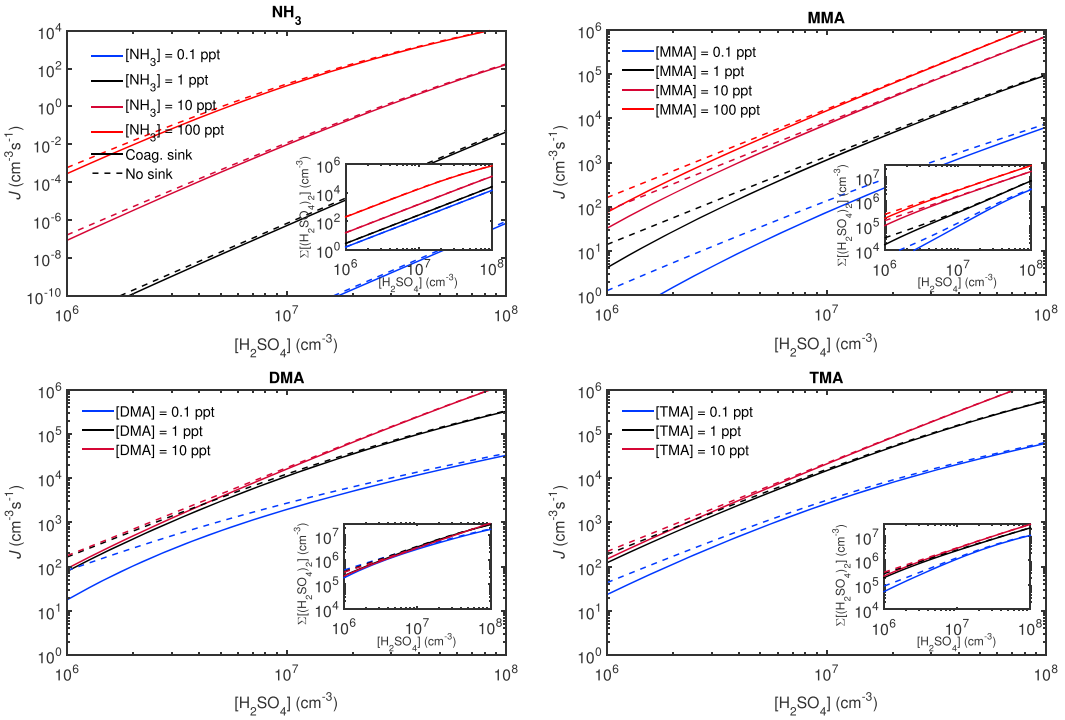

Figure 2. Simulated particle formation rate *J* out of the simulation system (the size over which *J* is determined is different for the studied bases because of the different sizes of the systems) as a function of monomer concentration at 278 K, RH = 38%, and a coagulation sink corresponding to average boundary layer conditions (equation (5)). The dashed lines show the formation rates with no coagulation losses, and the inset shows the steady state dimer concentration. Note that due to the relatively lower formation rates and dimer concentrations, the *y* axes for the ammonia system are different than for the other systems.

captured by the model. For DMA and TMA, the effect of sulfuric acid concentration compares well with the observations, while the dependence on base concentration is overpredicted. The increasing mismatch between the experimental and modeled base dependence as a function of base strength may be related to uncertainties in the centerline concentration of the base vapor: higher values of [base] make the simulated $\Sigma[(H_2SO_4)_2]$ less dependent on the base in the case of DMA and TMA (see Figure S15). The binding energy errors discussed in the previous section are also expected to affect the base dependence. Compared to high-level (CCSD(T)-F12a) results, the overestimation of the binding energy by the RICC2 method increases with the base strength (in the order $NH_3 < MMA < DMA < TMA$); on the other hand, destabilizing the clusters is expected to result in even stronger base dependence (Figure S11), suggesting that the differences to the observations are not primarily due to uncertainties in the energies.

For the H_2SO_4–DMA mixture, similar comparisons of observed and simulated dimer concentrations in the case of steady state conditions of a nucleation chamber experiment were previously presented by *Almeida et al.* [2013] and *Kupiainen-Määttä et al.* [2015]. In these comparisons, the absolute dimer concentration is somewhat overpredicted, while the dependence on $[H_2SO_4]$ is well reproduced and the dependence on [DMA] is slightly underpredicted (it must be kept in mind, however, that the comparisons are also likely to be affected by the different instruments and their settings used in the different experiments; see section 3.3). Altogether, the comparisons of Figure 1, as well as those shown in the previous works, demonstrate that the modeling tools used here are robust and capable of reliably describing the clustering dynamics in the studied H_2SO_4-base systems. The differences may be due to several sources of uncertainty related to both modeling and experimental data, discussed in section 3.3.

3.2. Steady State Formation Rates and Cluster Concentrations in Atmospheric Conditions

Figure 2 shows the steady state formation rate of particles growing out of the simulation systems and the sulfuric acid dimer concentrations as a function of monomer concentration at 278 K and RH = 38%. Such

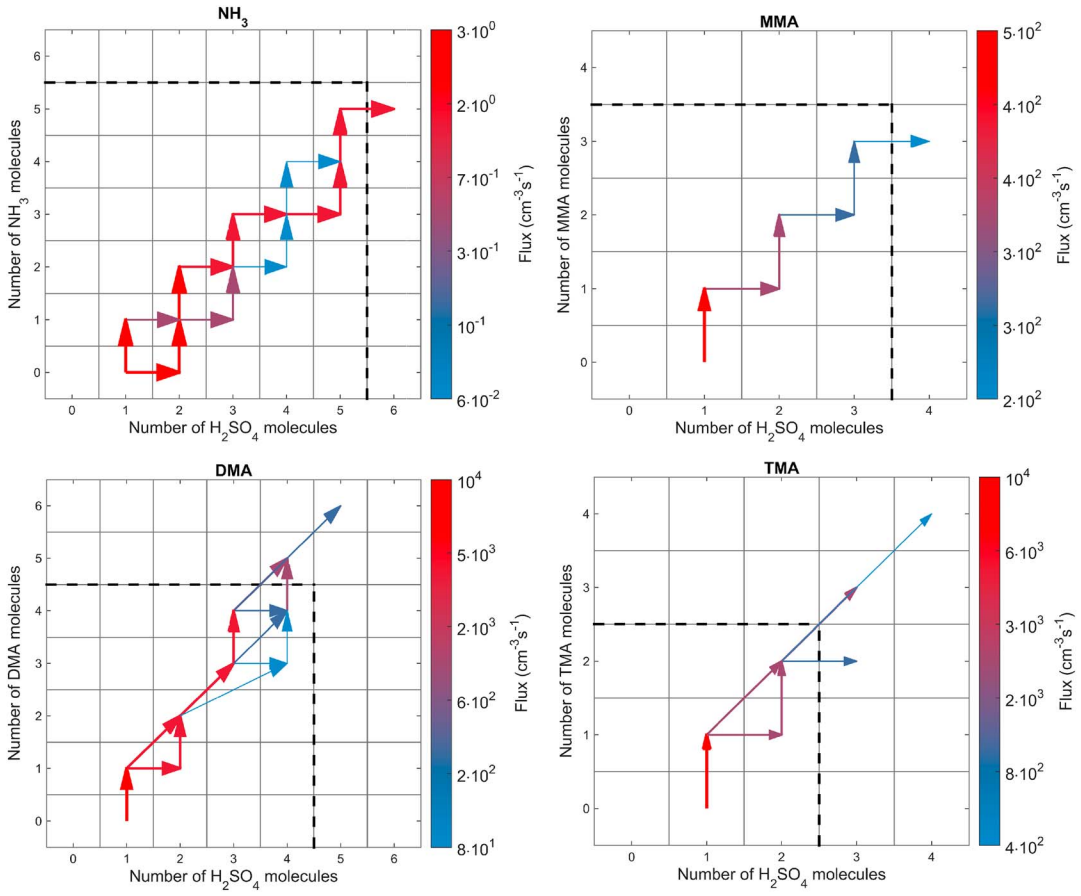

Figure 3. Main clustering pathways at $[H_2SO_4] = 5 \times 10^6$ cm^{-3}, [amine (NH_3)] = 1 (100) ppt ($3 \cdot 10^7$ ($3 \cdot 10^9$) cm^{-3}), T = 278 K, and RH = 38% (only pathways that are at least 5% of the net flux into the cluster are shown). The color and width of the arrows depict the relative magnitude of the particle flux in each system.

temperatures and RHs correspond to recent chamber experiments [e.g., *Almeida et al.*, 2013] and can be found in the boundary layer. The simulations were performed both in the presence and in the absence of a size-dependent coagulational scavenging sink (equation (5)).

The steady state simulations confirm the order of the stabilization capability of the studied bases suggested earlier: DMA $\geq$ TMA $>$ MMA $>$ NH_3. It can be noted that while the qualitative effect of the different bases on NPF is indicated by their relative proton affinities [see, e.g., *Ruusuvuori et al.*, 2013], the clustering efficiency is affected also by other factors. Although the gas-phase basicity of TMA is much higher than that of DMA, TMA does not bind significantly more strongly to sulfuric acid, and it is not more efficient in enhancing NPF, as it is able to form only one hydrogen bond. For DMA and TMA, the cluster formation is limited by the acid concentration at the studied conditions: the system becomes saturated with respect to base, and further increase in the base vapor has very little effect. In general, all amine cases yield roughly at least 10–10^3-fold dimer concentrations and at least 10^2–10^6-fold formation rates as compared to the simulations with ammonia as the base, with the differences increasing with decreasing vapor concentrations. At the studied conditions the effect of coagulation losses is overall quite small but nonnegligible at $[H_2SO_4] \lesssim 10^7$ cm^{-3}.

The growth pathways presented in Figure 3 depict the fundamental differences between the different bases: for the three amines, the first step of growth is the strong binding of a single acid molecule to a base molecule, whereas in the sulfuric acid-ammonia system, the acid molecule tends to bind to another acid instead of ammonia. For the studied amines, the initial growth step occurs virtually always via the H_2SO_4•base complex (that consists of one acid, one amine, and any number of water molecules); for the ammonia system, the acid dimer is more stable than the relatively weakly bound H_2SO_4•NH_3, and most (~90% in Figure 3) of the initial growth to $(H_2SO_4)_2$•NH_3 proceeds through $(H_2SO_4)_2$. For the strongest bases DMA and TMA, the

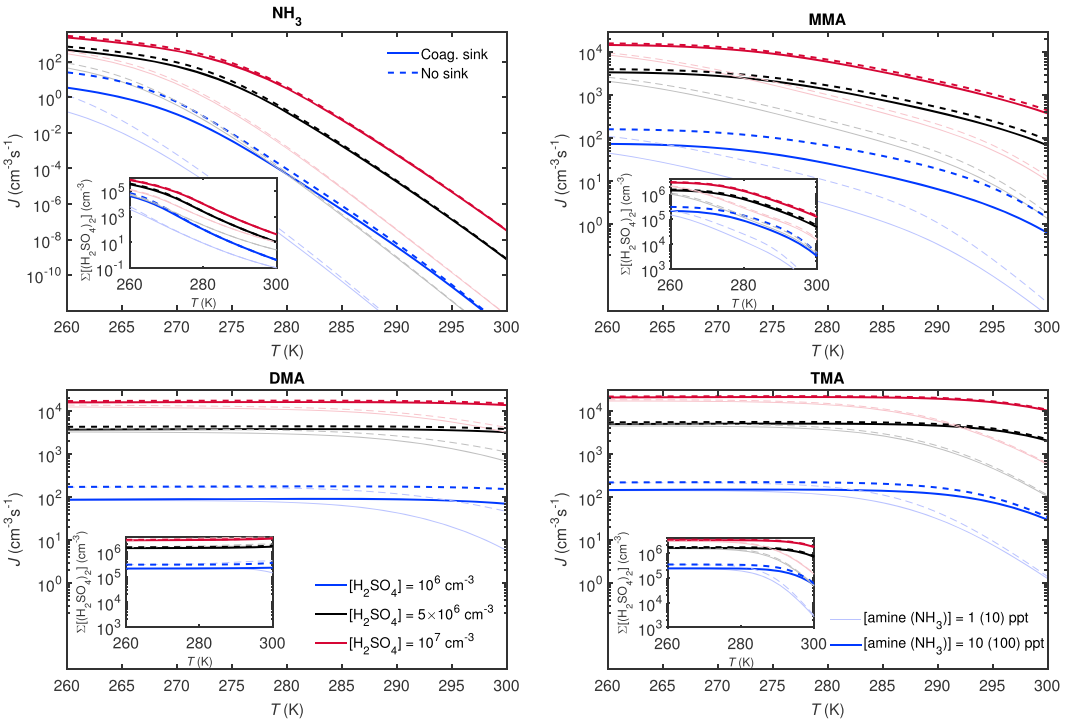

Figure 4. Simulated steady state formation rate *J* and dimer concentration as a function of temperature at RH = 38%.

concentration of H_2SO_4•base clusters is high enough for the cluster populations to grow also by collisions involving the H_2SO_4•base complex and possibly also larger clusters (Figure 3) in addition to the attachment of single molecules and their hydrates. This is in line with observations by *Lehtipalo et al.* [2016] and suggests that simplified growth schemes which consider only some of the kinetic processes can lead to significant uncertainties in describing the dynamics of different H_2SO_4-base systems.

3.2.1. Effect of Temperature

Figure 4 shows the temperature-dependent behavior of the formation rates and cluster concentrations in the range of 260–300 K. The formation of H_2SO_4-base clusters decreases drastically with increasing temperature for NH_3 and MMA. For TMA, the formation rate and dimer concentration remain unaltered up to ~280 K after which they start to decrease; for DMA *J* starts to decrease at ~290 K, while $\sum[(H_2SO_4)_2]$ very slightly increases, likely due to the reduced outgoing particle flux. The effect of increasing temperature is more prominent at the lower base concentrations ([amine (NH_3)] = 1 (10) ppt ($3 \cdot 10^7$ ($3 \cdot 10^8$) cm^{-3}); lighter lines) especially in the case of TMA. The temperature trends demonstrate the importance of quantitative understanding of cluster evaporation for assessing the response to ambient conditions: The more weakly bound systems are sensitive to the temperature, although the relative changes in the evaporation rate constants of individual clusters are of the same order as for the strongly binding systems (Figure S1 in the supporting information). When the absolute evaporation frequencies are very low compared to the collision frequencies, as for DMA and TMA, increases of even a couple of orders of magnitude in them do not have a large effect on the cluster concentrations.

In addition to the evaporation rate constants of individual clusters and their hydrates, the temperature can also affect the hydrate distributions and thus the relative contribution of different hydrates to the rate constants. For instance, the average number of water molecules decreases for clusters $(H_2SO_4)_2$ (~1 water less) and $(H_2SO_4)_2$•NH_3 (~0.5 waters less) as the temperature increases from 260 K to 300 K at RH = 38% (Figure S2 in the supporting information). For the H_2SO_4-amine clusters along the main growth pathways of the systems, the effect of temperature rise on cluster hydration is minor (Figure S2).

3.2.2. Effect of Relative Humidity

The effect of relative humidity on cluster formation is presented in Figure 5. Clusters containing the weaker bases NH_3 and MMA take up water more efficiently than DMA and TMA, and hydration stabilizes many of the

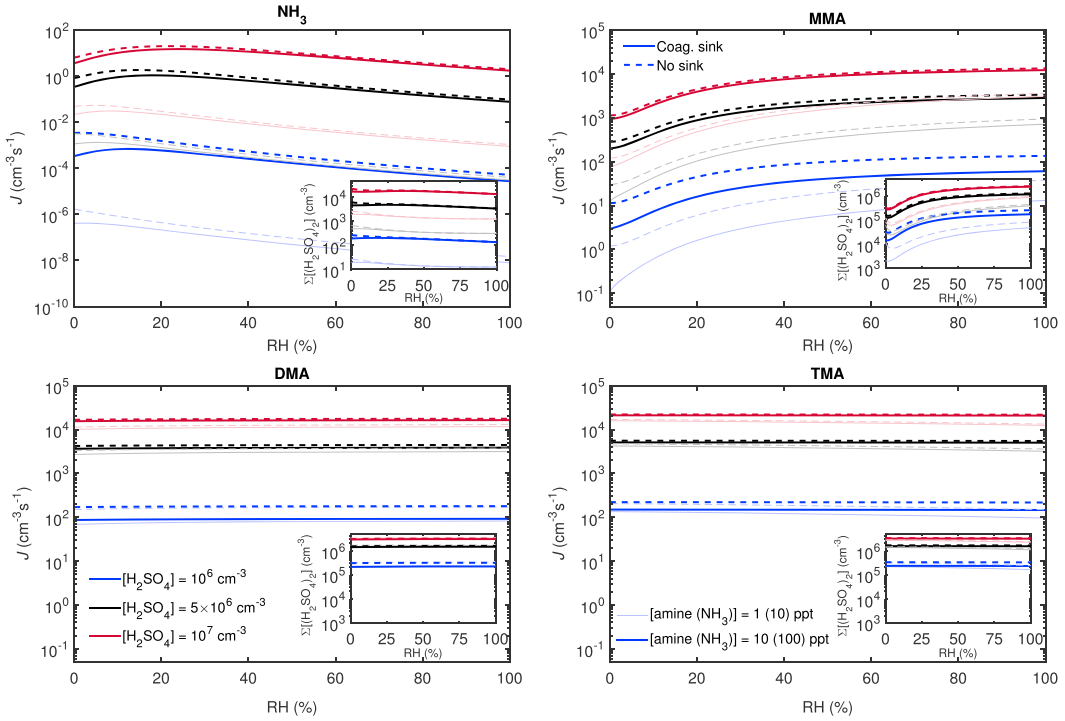

Figure 5. Simulated steady state formation rate *J* and dimer concentration as a function of relative humidity at 278 K.

key clusters in these systems leading to enhanced particle formation. On the other hand, some clusters become less stable with respect to the evaporation of H_2SO_4 and base molecules, and thus, hydration can also suppress net cluster formation as is the case for NH_3 at high RH. The effect depends on [H_2SO_4], [base] and temperature and can be considerably stronger at different conditions (for the detailed effects on *J*, see Figures S8 and S9). Stabilization of small clusters by hydration is most important for the H_2SO_4-MMA system, where *J* and $\sum[(H_2SO_4)_2]$ increase ~1 order of magnitude due to hydrate formation in the conditions of Figure 5. For DMA or TMA, the effect is insignificant: *J* and $\sum[(H_2SO_4)_2]$ are not notably affected by humidity in the studied conditions (see also Figures S8 and S9).

The effect of RH is due to changes in the effective evaporation rate constants of the key clusters, shown in Figure 6. As the evaporation rate constants can either increase or decrease due to hydration, the overall effects on the system dynamics can be complex. The collision rate constants increase monotonically as the collision cross sections increase, but the changes are very small [see *Henschel et al.*, 2016]. The scavenging rate constants slightly decrease due to lowered cluster mobility (roughly up to ~20% decrease at the studied conditions).

For NH_3, the most weakly bound clusters on the growth pathways in dry conditions (H_2SO_4•NH_3, $(H_2SO_4)_2$, $(H_2SO_4)_2$•$(NH_3)_2$, and $(H_2SO_4)_3$•NH_3) are stabilized by hydration, whereas the more tightly bound clusters ($(H_2SO_4)_2$•NH_3, $(H_2SO_4)_3$•$(NH_3)_2$, and $(H_2SO_4)_3$•$(NH_3)_3$) become slightly less stable against evaporation (Figure 6). The overall effect of humidity on the dimer concentration and formation rate is a nonlinear combination of the effects of changes in the stabilities of the key clusters. Thus, the resulting trend can vary according to the vapor concentrations which affect the growth routes (Figures S8 and S9). On the other hand, the growth routes can also be altered by changes in the effective rate constants (see Figure S10). For MMA, the evaporation rate constants are lower at higher RH except for $(H_2SO_4)_2$•MMA, which in any case has a low evaporation frequency (Figure 6). The small depression in the dimer concentration at RH ~5% is due to the almost unchanged evaporation rate constant of the H_2SO_4•MMA cluster in the region. The evaporation frequencies of DMA clusters have overall a slightly increasing trend with respect to RH, while the H_2SO_4•DMA complex is stabilized. H_2SO_4-TMA clusters, on the other hand, are destabilized by hydration relative to their respective evaporation products (Figure 6) and generally take up only very little water (Figures S3 and S7).

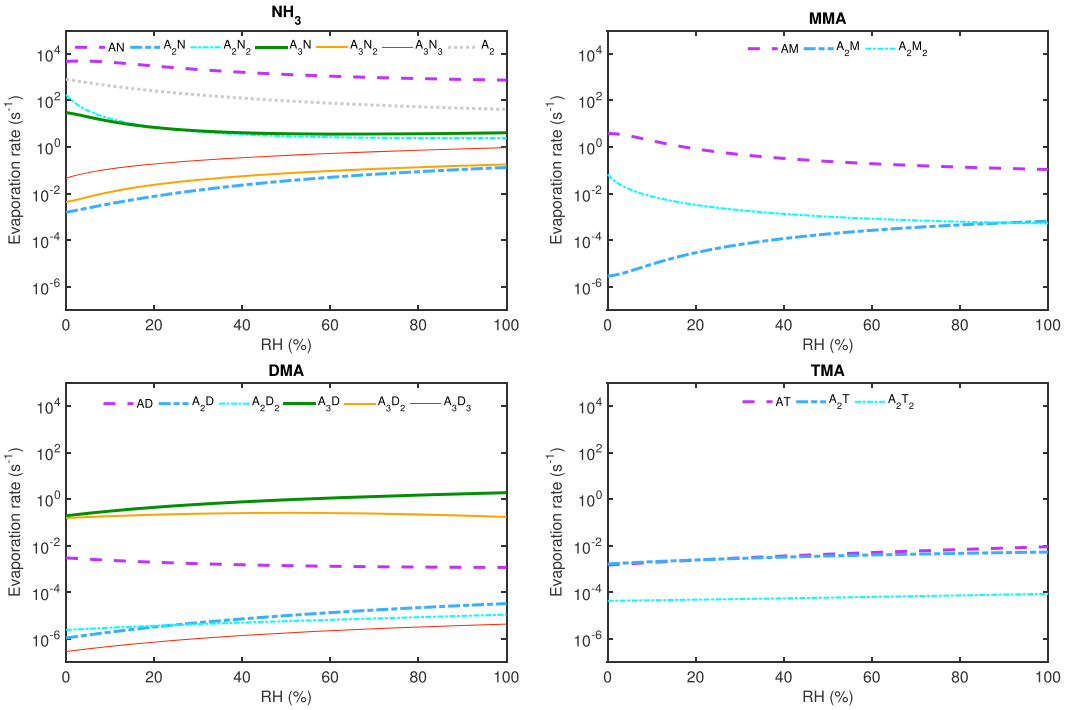

Figure 6. Effective total evaporation rate constants of individual clusters as a function of relative humidity at 278 K. Letters A, N, M, D, and T refer to H_2SO_4, NH_3, MMA, DMA, and TMA, respectively.

In general, hydration may have complicated, nonlinear effects on the dynamics of systems with significant cluster evaporation. On the other hand, for systems where the role of evaporation is minor, hydration does not have a strong effect. Similar conclusions have been deduced in the work by *Henschel et al.* [2016], where detailed discussions on the effect of water for particle formation from H_2SO_4 and NH_3 as compared to H_2SO_4 and DMA can be found.

3.3. Uncertainty Assessments

The largest source of uncertainty affecting the quantitative simulation results is the cluster free energies, on which the evaporation rate constants depend exponentially. To assess the effect of uncertainties in the stabilities of the very initial clusters, we performed test simulations using the CCSD(T)-F12a/VTZ-F12 electronic energies for the H_2SO_4•base clusters (for H_2SO_4•TMA for which the VTZ-F12 value could not be achieved, we used the VDZ-F12 value), shown in Figures S11 and S12. For the H_2SO_4-NH_3 system, the results do not change as the role of H_2SO_4•NH_3 is very minor. For MMA, the steady state formation rates and dimer concentrations decrease ~1–2 orders of magnitude. For DMA and TMA, J and $\sum[(H_2SO_4)_2]$ become clearly dependent on the amine concentration: at [amine] = 10 ppt ($3 \cdot 10^8$ cm^{-3}), there are no large differences compared to the RICC2/aug-cc-pV(T+d)Z results, but at the lower amine concentrations J and $\sum[(H_2SO_4)_2]$ decrease around 1–2 orders of magnitude depending on the vapor concentrations. For DMA, the overall growth pathways still include contributions from collisions with H_2SO_4•DMA and other clusters, while in the TMA system, cluster self-coagulation becomes negligible. However, otherwise, the qualitative results remain the same: the DMA and TMA systems behave similarly with respect to quantitative J and $\sum[(H_2SO_4)_2]$, while the MMA system shows weaker cluster formation. The principal first growth step in the amine systems is the formation of the H_2SO_4•base complex also with the CCSD(T)-F12a data. Changes in $\sum[(H_2SO_4)_2]$ are qualitatively similar for the flow tube simulations; however, the flow tube results and thus the comparison to the observations are affected also by hydration (the CCSD(T) energies were calculated only for dry clusters) and uncertainties in the base concentration (see below). In addition, the thermal contributions in the free energies involve uncertainties related to the rigid rotor-harmonic oscillator approximation, which may be comparable to the uncertainties in the electronic energies estimated based on the CCSD(T)-F12a calculations.

For the H_2SO_4-DMA system, we also performed simulations using data calculated at the PW91PW91/6-311++G(3df) level by *Nadykto et al*. [2014] as described in the supporting information. This data set predicts significantly weaker particle formation compared to the RICC2//B3LYP data and also to the experiments by *Jen et al*. [2014] (Figures S13 and S14), suggesting that the PW91PW91 values can be considered as lower limit estimates for the binding of H_2SO_4-DMA clusters.

In addition to evaporation rate constants, also, collision rate constants involve uncertainties: For instance, compared to hard-sphere collision rates used in this work, the collision constants between small clusters and molecules may be increased because of attractive forces due to permanent or induced dipoles. Test simulations performed with all collision constants increased by a factor of 2 showed an approximately twofold to fivefold increase in the formation rates for all studied systems, but the relative differences between the different bases were not affected.

Comparisons with cluster measurements involve also various experimental uncertainties: determining the cluster-dependent transmission efficiency of the mass spectrometers and converting signal counts to concentrations is not straightforward [see, e.g., *Jen et al*., 2014]. Different instrumental settings can affect the detected distribution via effects on cluster transmission and fragmentation [e.g., *Schobesberger et al*., 2013], which should be kept in mind when comparing observations to modeled concentrations. In case of flow tube experiments, the measurement result may be affected also by nonuniform mixing of the species in the sample flow due to, e.g., strong radial gradients which affect the loss rate constants from the central streamline (Figure S15). Further, the sample measured from a laminar flow consists of clusters with a range of residence times. Examination of the time-dependent cluster concentrations in simulations corresponding to the flow tube of *Jen et al*. [2014] suggests that changes in the residence time may play a nonnegligible role (Figure S16). Computational fluid dynamics applications are currently being developed to resolve the details of flow tube setups [*Hanson et al*., 2017].

4. Conclusions

The potential role of different alkylamines in atmospheric new particle formation (NPF) involving sulfuric acid and water was explored by simulations of molecular cluster formation in a range of ambient conditions relevant to the lower troposphere. The capabilities of amines to stabilize small clusters of sulfuric acid have previously been assessed by quantum chemical calculations on cluster formation thermodynamics. In this work, we applied quantum chemical data in cluster population dynamics simulations to yield cluster concentrations and formation rates, which provide information on the stabilization potential of different compounds in the form of quantities that can be measured or directly applied in atmospheric NPF modeling.

It is established that amines generally enhance sulfuric acid-driven NPF more than the most abundant base precursor ammonia; the detailed effects, however, depend on the amine type. The relative stabilization efficiencies of monomethylamine, dimethylamine, and dimethylamine (MMA, DMA, and TMA) in terms of cluster formation are in line with previous observations in laboratory experiments: the stabilizing strength of the amines with respect to each other and ammonia is DMA $\geq$ TMA $>$ MMA $>$ NH_3. The studied bases can be roughly divided into two categories: the stronger stabilizers DMA and TMA form stable H_2SO_4-base clusters for which evaporation is suppressed, while clusters of the weaker bases MMA and NH_3 evaporate significantly. As the evaporation rate constants depend on the temperature and relative humidity, the absolute cluster concentrations and formation rates in systems of the weaker stabilizers are more sensitive to variations in these ambient conditions.

While temperature has a straightforward, lowering effect on cluster formation rates, the effect of hydration is more complex and depends on the amine. DMA clusters become partly hydrated with increasing RH, but the effect on cluster stability is very minor. Small TMA clusters take up only very little water and become destabilized against evaporation with increasing humidity. For DMA and TMA, the overall effect of hydration is small; cluster formation involving MMA, on the other hand, is generally enhanced by water in the studied conditions.

These findings address the question of what level of simplification is justifiable in atmospheric NPF modeling: using a surrogate amine species is beneficial for, e.g., large-scale models with less detailed chemistry. The presented results point to approximating DMA and TMA as a lumped species being a reasonable approach

if a detailed description is not required or affordable: cluster formation and its response to changes in the ambient temperature and relative humidity are roughly similar for them. MMA enhances particle formation less than DMA and TMA, and the qualitative trends often resemble those of ammonia rather than those of the stronger amines. For detailed process modeling, including interpretation of laboratory experiments, MMA cannot be approximated as DMA and TMA. For large-scale modeling of NPF, on the other hand, the significant differences in the formation rates may not lead to notable changes in cloud condensation nuclei (CCN) concentrations due to possible feedbacks between nanoparticle formation and growth to much larger sizes given that the formation rate for MMA is nonnegligible [*Westervelt et al*., 2014]. Differences in concentrations of much larger particles and CCN can be mainly expected for conditions where particle formation rate for DMA and TMA is significant (>1 cm^{-3} s^{-1}) and for MMA negligible ($\ll 1$ cm^{-3} s^{-1}), namely, at lower [H_2SO_4], [amine], and RH and higher boundary layer temperatures (in the simulations of this work, approximately at [H_2SO_4] = ~10^6 cm^{-3}, [amine] = ~1 ppt (~10^7 cm^{-3}), RH $\lesssim$ 20%, and temperatures of $\gtrsim$ 290 K). In these conditions, including MMA emissions in a NPF scheme which assumes the clustering properties of DMA and TMA can be considered to give an upper limit for H_2SO_4-amine-based particle formation, which should be borne in mind when interpreting model results.

As a final remark, as amines form strongly bound complexes with sulfuric acid, cluster self-coagulation is likely to be nonnegligible for the kinetics of H_2SO_4-amine systems. This makes theoretical nucleation schemes considering only cluster-monomer interactions, such as approaches based on the classical nucleation theory, not valid for these systems: solving the particle formation rate requires more sophisticated treatment of the clustering dynamics.

Acknowledgments
The data used are available in the figures, tables, supporting information, and cited references. ERC projects 278277-ATMOGAIN, 257360-MOCAPAF, and 692891-DAMOCLES; Formas project 2015-749; the Academy of Finland Center of Excellence program project 272041; and National Science Foundation AGS project 1524211 are acknowledged for funding. The authors thank CSC-IT Center for Science in Espoo, Finland, for computing time.

References

Ahlrichs, R., M. Bär, M. Häser, H. Horn, and C. Kölmel (1989), Electronic structure calculations on workstation computers: The program system Turbomole, *Chem. Phys. Lett.*, *162*, 165–169.

Almeida, J., et al. (2013), Molecular understanding of sulphuric acid-amine particle nucleation in the atmosphere, *Nature*, *502*, 359–363.

Belman, N., J. N. Israelachvili, Y. Li, C. R. Safinya, J. Bernstein, and Y. Golan (2009), The temperature-dependent structure of alkylamines and their corresponding alkylammonium-alkylcarbamates, *J. Am. Chem. Soc.*, *131*, 9107–9113, doi:10.1021/ja902944t.

Bergman, T., A. Laaksonen, H. Korhonen, J. Malila, E. M. Dunne, T. Mielonen, K. E. J. Lehtinen, T. Kühn, A. Arola, and H. Kokkola (2015), Geographical and diurnal features of amine-enhanced boundary layer nucleation, *J. Geophys. Res. Atmos.*, *120*, 9606–9624, doi:10.1002/2015JD023181.

Bustos, D. J., B. Temelso, and G. C. Shields (2014), Hydration of the sulfuric acid-methylamine complex and implications for aerosol formation, *J. Phys. Chem. A*, *118*, 7430–7441, doi:10.1021/jp500015t.

Crane (1982), Flow of fluids through valves, fittings, and pipe, Tech. Paper No. 410 M, Crane Co.

Dal Maso, M., A. Hyvärinen, M. Komppula, P. Tunved, V.-M. Kerminen, H. Lihavainen, Y. Viisanen, H.-C. Hansson, and M. Kulmala (2008), Annual and interannual variation in boreal forest aerosol particle number and volume concentration and their connection to particle formation, *Tellus B*, *60*, 495–508.

DePalma, J. W., D. J. Doren, and M. V. Johnston (2014), Formation and growth of molecular clusters containing sulfuric acid, water, ammonia, and dimethylamine, *J. Phys. Chem. A*, *118*, 5464–5473, doi:10.1021/jp503348b.

Erupe, M. E., A. A. Viggiano, and S.-H. Lee (2011), The effect of trimethylamine on atmospheric nucleation involving H_2SO_4, *Atmos. Chem. Phys.*, *11*, 4767–4775.

Frisch, M. J., et al. (2009), *Gaussian 09 Revision D.01*, Gaussian Inc., Wallingford Conn.

Ge, X., A. S. Wexler, and S. L. Clegg (2011), Atmospheric amines—Part I. A review, *Atmos. Environ.*, *45*, 524–546.

Glasoe, W. A., K. Volz, B. Panta, N. Freshour, R. Bachman, D. R. Hanson, P. H. McMurry, and C. Jen (2015), Sulfuric acid nucleation: An experimental study of the effect of seven bases, *J. Geophys. Res. Atmos.*, *120*, 1933–1950, doi:10.1002/2014JD022730.

Hanson, D. R., I. Bier, B. Panta, C. N. Jen, and P. H. McMurry (2017), Computational fluid dynamics studies of a flow reactor: Free energies of clusters of sulfuric acid with NH_3 or dimethyl amine, *J. Phys. Chem. A*, *121*, 3976–3990, doi:10.1021/acs.jpca.7b00252.

Haynes, W. M. (Ed.) (2014), *CRC Handbook of Chemistry and Physics*, 94th ed., (Internet Version), CRC Press/Taylor and Francis, Boca Raton, Fla.

Henschel, H., T. Kurtén, and H. Vehkamäki (2016), Computational study on the effect of hydration on new particle formation in the sulfuric acid/ammonia and sulfuric acid/dimethylamine systems, *J. Phys. Chem. A*, *120*, 1886–1896, doi:10.1021/acs.jpca.5b11366.

Henschel, H., J. C. A. Navarro, T. Yli-Juuti, O. Kupiainen-Määttä, T. Olenius, I. K. Ortega, S. L. Clegg, T. Kurtén, I. Riipinen, and H. Vehkamäki (2014), Hydration of atmospherically relevant molecular clusters: Computational chemistry and classical thermodynamics, *J. Phys. Chem. A*, *118*, 2599–2611.

Jen, C. N., P. H. McMurry, and D. R. Hanson (2014), Stabilization of sulfuric acid dimers by ammonia, methylamine, dimethylamine, and trimethylamine, *J. Geophys. Res. Atmos.*, *119*, 7502–7514, doi:10.1002/2014JD021592.

Karton, A. (2016), A computational chemist's guide to accurate thermochemistry for organic molecules, *Wiley Interdiscip. Rev. Comput. Mol. Sci.*, *6*, 292–310, doi:10.1002/wcms.1249.

Kupiainen, O., I. K. Ortega, T. Kurtén, and H. Vehkamäki (2012), Amine substitution into sulfuric acid—Ammonia clusters, *Atmos. Chem. Phys.*, *12*, 3591–3599.

Kupiainen-Määttä, O., H. Henschel, T. Kurtén, V. Loukonen, T. Olenius, P. Paasonen, and H. Vehkamäki (2015), Comment on 'Enhancement in the production of nucleating clusters due to dimethylamine and large uncertainties in the thermochemistry of amine-enhanced nucleation ' by Nadykto et al, Chem. Phys. Lett. 609 (2014) 42-49, *Chem. Phys. Lett.*, *624*, 107–110, doi:10.1016/j.cplett.2015.01.029.

Kupiainen-Määttä, O., T. Olenius, T. Kurtén, and H. Vehkamäki (2013), CIMS sulfuric acid detection efficiency enhanced by amines due to higher dipole moments: A computational study, *J. Phys. Chem. A*, *117*, 14,109–14,119.

Kürten, A., A. Bergen, M. Heinritzi, M. Leiminger, V. Lorenz, F. Piel, M. Simon, R. Sitals, A. C. Wagner, and J. Curtius (2016), Observation of new particle formation and measurement of sulfuric acid, ammonia, amines and highly oxidized organic molecules at a rural site in central Germany, *Atmos. Chem. Phys.*, *16*, 12,793–12,813, doi:10.5194/acp-16-12793-2016.

Kürten, A., et al. (2014), Neutral molecular cluster formation of sulfuric acid-dimethylamine observed in real time under atmospheric conditions, *Proc. Natl. Acad. Sci. U.S.A.*, *111*, 15,019–15,024, doi:10.1073/pnas.1404853111.

Kurtén, T., V. Loukonen, H. Vehkamäki, and M. Kulmala (2008), Amines are likely to enhance neutral and ion-induced sulfuric acid-water nucleation in the atmosphere more effectively than ammonia, *Atmos. Chem. Phys.*, *8*, 4095–4103, doi:10.5194/acp-8-4095-2008.

Lane, J. R., and H. G. Kjaergaard (2009), Explicitly correlated intermolecular distances and interaction energies of hydrogen bonded complexes, *J. Chem. Phys.*, *131*, doi:10.1063/1.3159672.

Lehtinen, K. E. J., M. Dal Maso, M. Kulmala, and V.-M. Kerminen (2007), Estimating nucleation rates from apparent particle formation rates and vice versa: Revised formulation of the Kerminen-Kulmala equation, *J. Aerosol Sci.*, *38*, 988–994.

Lehtipalo, K., et al. (2016), The effect of acid-base clustering and ions on the growth of atmospheric nano-particles, *Nat. Commun.*, *7*, doi:10.1038/ncomms11594.

Lemmon, E. W., and R. T. Jacobsen (2004), Viscosity and thermal conductivity equations for nitrogen, oxygen, argon, and air, *Int. J. Thermophys.*, *25*, 21–69, doi:10.1023/B:IJOT.0000022327.04529.f3.

Leverentz, H. R., J. I. Siepmann, D. G. Truhlar, V. Loukonen, and H. Vehkamäki (2013), Energetics of atmospherically implicated clusters made of sulfuric acid, ammonia, and dimethyl amine, *J. Phys. Chem. A*, *117*, 3819–3825.

Loukonen, V., T. Kurtén, I. K. Ortega, H. Vehkamäki, A. A. H. Padua, K. Sellegri, and M. Kulmala (2010), Enhancing effect of dimethylamine in sulfuric acid nucleation in the presence of water—A computational study, *Atmos. Chem. Phys.*, *10*, 4961–4974.

Lv, S.-S., S.-K. Miao, Y. Ma, M.-M. Zhang, Y. Wen, C.-Y. Wang, Y.-P. Zhu, and W. Huang (2015), Properties and atmospheric implication of methylamine—Sulfuric acid-water clusters, *J. Phys. Chem. A*, *119*, 8657–8666, doi:10.1021/acs.jpca.5b03325.

Myllys, N., J. Elm, and T. Kurtén (2016), Density functional theory basis set convergence of sulfuric acid-containing molecular clusters. *Comput. Theor. Chem.*, *1098*, 1–12.

Nadykto, A. B., F. Yu, M. V. Jakovleva, J. Herb, and Y. Xu (2011), Amines in the Earth's atmosphere: A density functional theory study of the thermochemistry of pre-nucleation clusters, *Entropy*, *13*, 554–569.

Nadykto, A. B., J. Herb, F. Yu, and Y. Xu (2014), Enhancement in the production of nucleating clusters due to dimethylamine and large uncertainties in the thermochemistry of amine-enhanced nucleation, *Chem. Phys. Lett.*, *609*, 42–49.

Olenius, T., O. Kupiainen-Määttä, I. K. Ortega, T. Kurtén, and H. Vehkamäki (2013), Free energy barrier in the growth of sulfuric acid-ammonia and sulfuric acid-dimethylamine clusters, *J. Chem. Phys.*, *139*, doi:10.1063/1.4819024.

Olenius, T., T. Kurtén, O. Kupiainen-Määttä, H. Henschel, I. K. Ortega, and H. Vehkamäki (2014), Effect of hydration and base contaminants on sulfuric acid diffusion measurement: A computational study, *Aerosol Sci. Technol.*, *48*, 593–603, doi:10.1080/02786826.2014.903556.

Ortega, I. K., O. Kupiainen, T. Kurtén, T. Olenius, O. Wilkman, M. J. McGrath, V. Loukonen, and H. Vehkamäki (2012), From quantum chemical formation free energies to evaporation rates, *Atmos. Chem. Phys.*, *12*, 225–235.

Ortega, I. K., T. Olenius, O. Kupiainen-Määttä, V. Loukonen, T. Kurtén, and H. Vehkamäki (2014), Electrical charging changes the composition of sulfuric acid-ammonia/dimethylamine clusters, *Atmos. Chem. Phys.*, *14*, 7995–8007.

Paasonen, P., et al. (2012), On the formation of sulphuric acid—Amine clusters in varying atmospheric conditions and its influence on atmospheric new particle formation, *Atmos. Chem. Phys.*, *12*, 9113–9133.

Qiu, C., and R. Zhang (2013), Multiphase chemistry of atmospheric amines, *Phys. Chem. Chem. Phys.*, *15*, 5738–5752.

Ruusuvuori, K., T. Kurtén, I. K. Ortega, J. Faust, and H. Vehkamäki (2013), Proton affinities of candidates for positively charged ambient ions in boreal forests, *Atmos. Chem. Phys.*, *13*, 10,397–10,404, doi:10.5194/acp-13-10397-2013.

Schobesberger, S., et al. (2013), Molecular understanding of atmospheric particle formation from sulfuric acid and large oxidized organic molecules, *Proc. Natl. Acad. Sci. U.S.A.*, *110*, 17,223–17,228.

Werner, H.-J., et al. (2012), MOLPRO, version 2012.1, a package of ab initio programs. [Available at http://www.molpro.net.]

Westervelt, D. M., J. R. Pierce, and P. J. Adams (2014), Analysis of feedbacks between nucleation rate, survival probability and cloud condensation nuclei formation, *Atmos. Chem. Phys.*, *14*, 5577–5597, doi:10.5194/acp-14-5577-2014.

Yu, H., R. McGraw, and S.-H. Lee (2012), Effects of amines on formation of sub-3 nm particles and their subsequent growth, *Geophys. Res. Lett.*, *39*, L02807, doi:10.1029/2011GL050099.

Zhao, J., J. N. Smith, F. L. Eisele, M. Chen, C. Kuang, and P. H. McMurry (2011), Observation of neutral sulfuric acid-amine containing clusters in laboratory and ambient measurements, *Atmos. Chem. Phys.*, *11*, 10,823–10,836, doi:10.5194/acp-11-10823-2011.